

Seismic Behavior of Reinforced Concrete Piles under Ground

Takeshi Maki¹ and Hiroshi Mutsuyoshi²

Received 6 July 2003, accepted 1 December 2003

Abstract

This paper reports the results of experimental and analytical investigation on the response behavior of reinforced concrete piles under ground. From the experimental results, it was clarified that the axial load at pile head affects the restoring force degradation and the maximum damage point is dependent on the relative stiffness between the pile and surrounding soil. From the analytical study using 3-dimensional FEM analysis, the experimental behavior could be adequately simulated by the applied method. Further investigations on the shapes or areas of hysteresis loops will be needed for the future application of this method to seismic performance evaluation of the entire structure-pile foundation-soil system.

1. Introduction

The Hyogoken Nanbu Earthquake of 1995 caused serious damage not only to many reinforced concrete structures but also to their foundations under ground. Subsequent investigations demonstrated the adequacy of practical seismic design methods taking into account absorbed energy in the plastic deformation range of reinforced concrete members, and based on these results, seismic retrofitting has been widely performed to achieve high ductility of existing RC structures. However, retrofitting some components of the structural system including, in the cases of bridges, piers, girders, bearings, footings and piles, may cause damage to another components or members in the system during the next severe earthquake. In order to clarify and evaluate such a mechanism, it is essential to develop seismic performance evaluation techniques for entire RC structural systems with careful consideration of the effect of soil-structure interactions (Fukui et al. 1998, Chai et al. 2002). The recent seismic design code of concrete structures (JSCE 2002) prescribes a response analysis method for strong seismic motion, whereby the structure in question should be modeled with its foundation and surrounding soil, and the design seismic wave should be input to the model from its engineering base in time domain. In this method, careful evaluation of analytical results would be needed while considering possible errors of modeling, parameters and calculation, especially in a large deformation range of members and soil, because there is no clear concept of a modeling method of foundation and soil, and little identification of the precise behavior of foundations during earthquakes.

The objective of this paper is to clarify the behavior

of reinforced concrete piles surrounded by a soil media when the piles are subjected to a large plastic deformation. For this purpose, several loading tests of reinforced concrete piles were conducted in order to achieve not only a good understanding of pile behaviors but also a set of data that can be utilized for subsequent analytical investigations (Maki et al. 2000, Maki et al. 2002).

2. Experimental procedure

2.1 Experimental setup for cyclic loading tests

When a pile foundation is subjected to seismic waves, there are two factors that dominate its behavior. The first one is the inertial force of the superstructure that acts at the pile head as axial and horizontal force, and moment. The other is the inertial force that acts as non-proportional distributed lateral force. Focusing on the former, lateral loading tests of pile were conducted in order to clarify the restoring force and deformation of pile in soil media. **Figure 1** and **2** show the experimen-

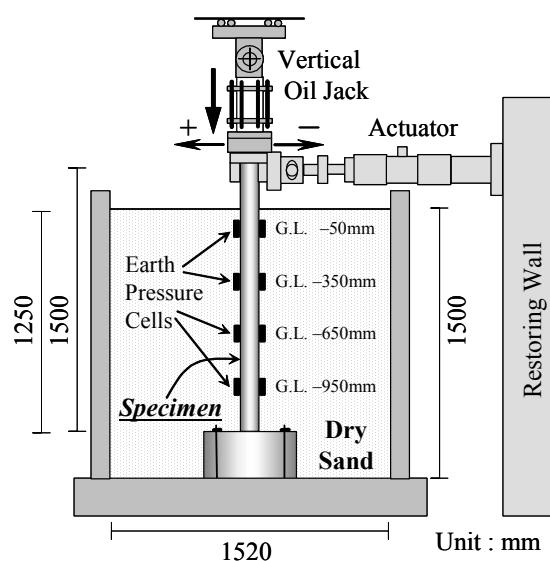


Fig. 1 Setup for loading tests.

¹Research Associate, Department of Civil and Environmental Engineering, Saitama University, Japan.
E-mail: maki@p.mtr.civil.saitama-u.ac.jp

²Professor, Department of Civil and Environmental Engineering, Saitama University, Japan

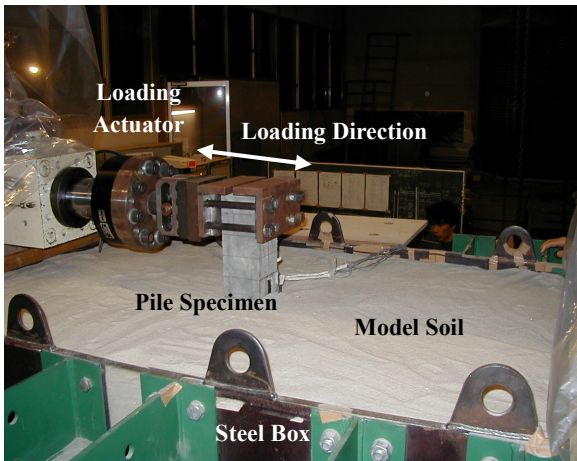


Fig. 2 Loading system.

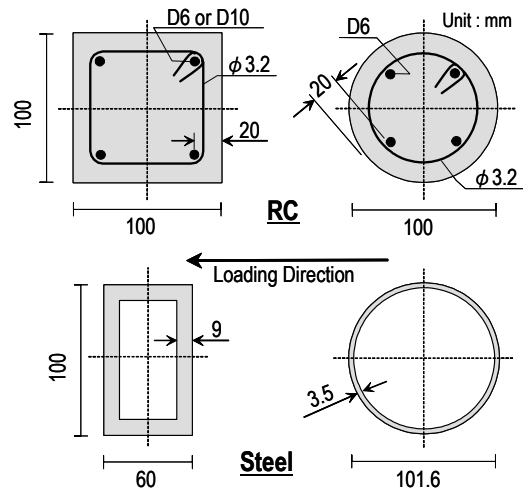


Fig. 3 Cross sectional shape of specimens.

Table 1 Experimental variables.

Case	Pile Specimen				Condition at Pile Head	Axial Stress (MPa)	Model Soil		
	Material	Cross Sectional Shape	Longitudinal Reinf. Ratio	Comp. Strength of Concrete (MPa)			Condition	Relative Density	
RX-0-L	RC	Rectangle	2.85%	43.0	Rotation Free	0	Loose	55.5%	
RR-0-L				45.3		0		55.5%	
RR-2-L				46.6		2		55.5%	
RR-0-D			1.27%	42.3		Rotation Free	0	Dense	70.3%
RR-2-D				45.5			2		83.2%
RR-4-D				52.6			4		86.4%
RR-V-D				40.8			0~4		87.1%
RR-C-D				43.5			2		88.7%
RC-0-D			Circular	1.61%		44.3	Rotation Free	0	Loose
SR-0-L	Steel	Rectangle	-	-	Rotation Free	0	Loose	55.5%	
SR-0-D						0		Dense	73.5%
SR-2-D						2	Dense		90.5%
SC-0-D						0		67.3%	

tal loading system. RC pile specimens were fixed to a rigid steel box, and the box was filled with a dry sand soil. Horizontal reversed cyclic displacements were applied under constant vertical loads through a loading actuator. Deformations and soil pressures of the concerned parts of the specimens were measured using strain gauges and earth pressure cells attached to the pile surfaces.

2.2 Experimental variables

The experimental variables for RC pile specimens included the sectional shape, reinforcement ratio, soil stiffness, conditions at pile head and vertical stress level. In addition, four types of steel pile specimens were tested for checking soil pressures on the pile surfaces. All experimental cases are listed in **Table 1**. Each specimen had an equal width of 100 mm perpendicular to the loading direction. For RC pile specimens, four deformed bars (6 mm or 10 mm in diameter) were arranged as longitudinal reinforcement in the section, and

round bars of 3.2 mm in diameter were used with 100 mm spacing for lateral reinforcement. The dimensions of cross sections and arrangement of reinforcing bars are illustrated in **Fig. 3**. The applied vertical stress levels were 0MPa, 2MPa and 4MPa. These values were defined as allowable bearing stresses under normal and

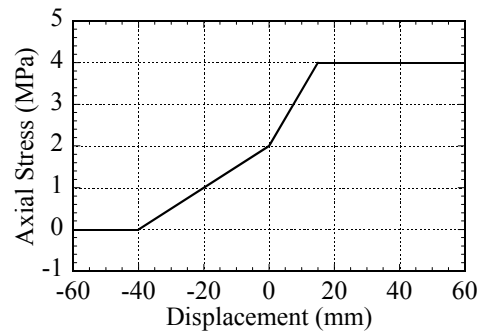


Fig. 4 Pattern for varying axial stress.

Table 2 Mechanical properties of all specimens.

Case	Initial Stiffness (10 ¹⁰ N*mm ²)	Yield Stiffness (10 ¹⁰ N*mm ²)	Yield Moment (10 ⁶ N*mm)	Yield Curvature (micro/mm)	Ultimate Moment (10 ⁶ N*mm)	Ultimate Curvature (micro/mm)
RX-0-L	34.829	10.379	3.975	38.3	4.010	175.8
RR-0-L	33.380	5.609	2.025	36.1	2.053	252.5
RR-2-L	31.969	7.512	3.045	40.5	3.257	182.5
RR-0-D	31.294	5.453	1.985	36.4	2.015	245.2
RR-2-D	32.092	7.498	3.048	40.6	3.259	182.9
RR-4-D	36.759	8.818	3.771	42.8	4.002	166.4
RR-V-D	28.999	7.238	3.007	41.5	3.198	171.8
RR-C-D	31.786	7.402	3.039	41.1	3.244	180.3
RC-0-D	19.647	3.375	1.583	46.9	1.560	180.4
Case	Initial Stiffness (10 ¹⁰ N*mm ²)	Moment of Inertia (10 ⁶ mm ⁴)	Yield Moment (10 ⁶ N*mm)	Yield Curvature (micro/mm)		
SR-0-L	20.813	1.297	17.297	83.1		
SR-0-D						
SR-2-D			10.213	49.1		
SC-0-D						

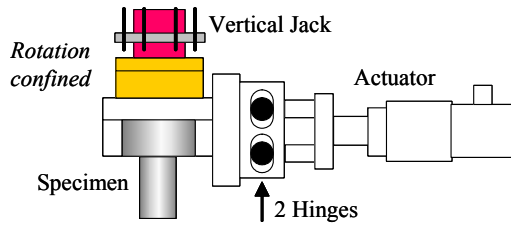


Fig. 5 Configuration for RC-C-D.

Table 3 Specification of Gifu sand.

Specific Gravity	2.643
Maximum Diameter D _{max} (mm)	0.84
60% Diameter D ₆₀ (mm)	0.35
30% Diameter D ₃₀ (mm)	0.31
10% Diameter D ₁₀ (mm)	0.22
Coefficient of Uniformity U _c	1.59
Maximum Void Ratio e _{max}	1.126
Minimum Void Ratio e _{min}	0.717

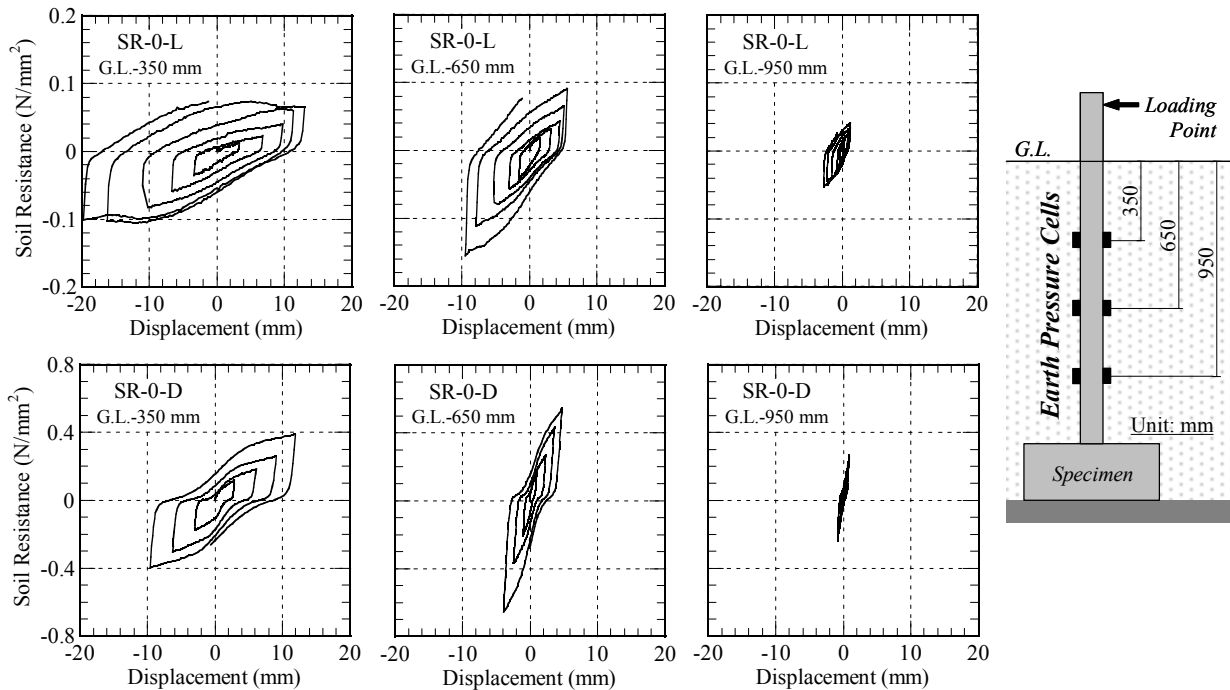


Fig. 6 Subgrade reactions of soil (SR-0-L and SR-0-D).

seismic conditions. In addition, variable vertical stresses between 0MPa and 4MPa were applied in RR-V-D in proportion to the horizontal displacement at the pile head, as shown in Fig. 4. The additional case of a specimen with rotation-fixed pile head condition was

conducted (RR-C-D). The specimen for this case had a small footing at its top and the footing was subjected to horizontal displacements through a two-hinge swivel head, as shown in Fig. 5. In addition, loading tests of steel pile specimens with rectangle and circular sections,

having the same initial stiffness, were conducted for checking elastic deformations and subgrade soil reactions. The mechanical properties of all the specimens are listed in **Table 2**. Dry sand consisting of uniform diameter particles was used in the experiments. The properties of the used sand are shown in **Table 3**. The soil stiffness was included in the experimental variables, which was realized by controlling the relative density of the model soil.

These experimental conditions are defined as close to the real conditions as possible, but further different conditions are also included. For example, soil deformation is perfectly confined by a steel box, or pile specimen is perfectly fixed to the bottom of a steel box. These peculiar conditions were established with the intention of providing clear boundary conditions for the subsequent

analytical investigations. Concerning the scale of a rigid steel box, the distance from the specimen to the wall of the box is about seven times the diameter of the specimen, in order to decrease the effect of wall confinement on the behavior of specimens. In addition, the depth of the rigid steel box is more than ten times the pile diameter. Therefore, these experimental conditions model a real RC pile 1 m in diameter and 10 m in length embedded in substantially soft soil.

3. Test results

3.1 Subgrade reactions of soil

In the cases of SR-0-L and SR-0-D, longitudinal strains of the pile surface were measured at ten measuring points along the pile axis. The horizontal displacements

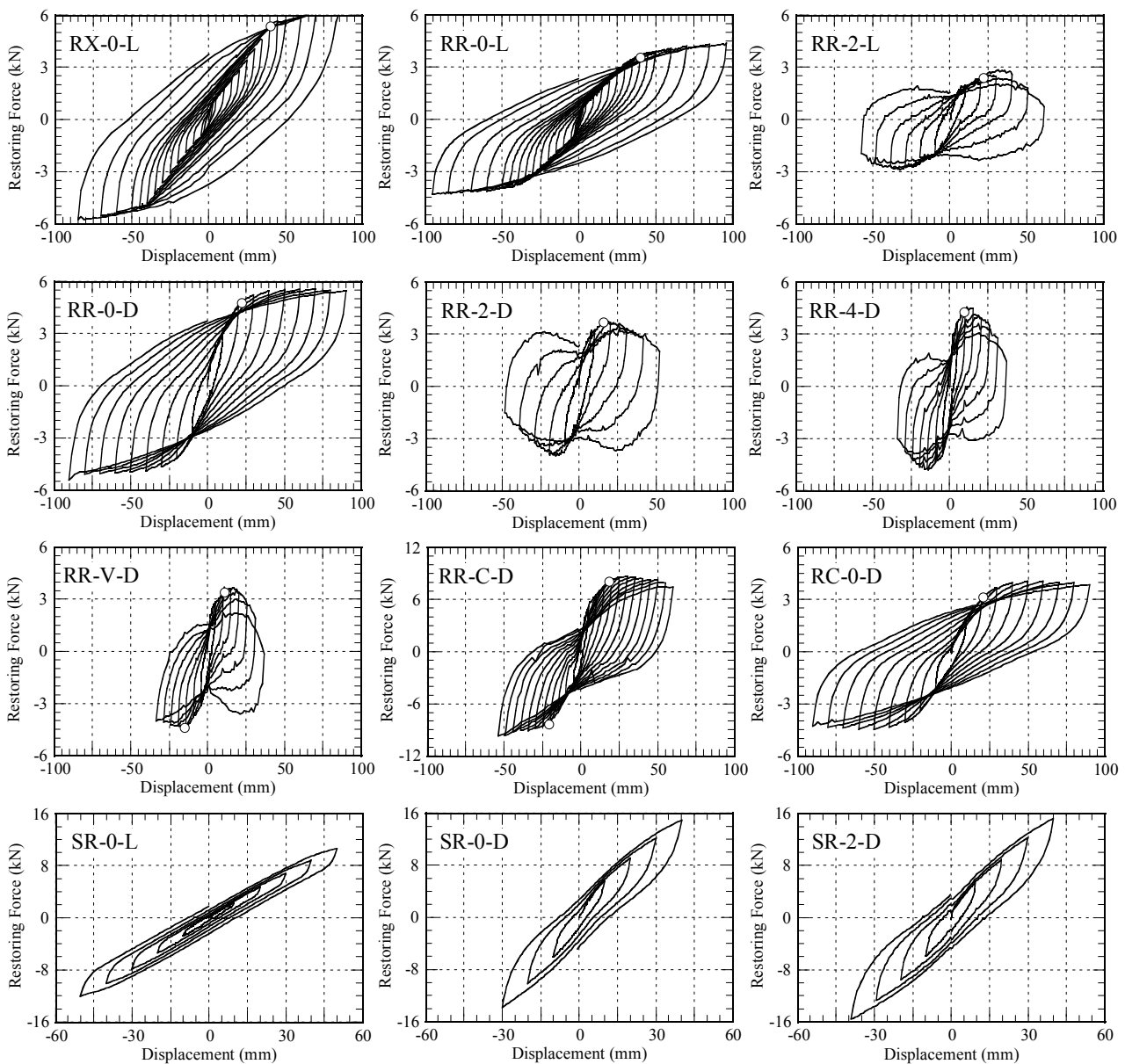


Fig. 7 Restoring force - displacement hysteresis curves (o : Yielding point) .

at the depths at which earth pressure cells were attached were calculated at each loading step by integrating a curvature distribution whereby the scattered values of curvature obtained from the measured strains were approximated by a cubic spline function. The relationships between measured soil pressures (that is, subgrade reactions of soil) and calculated horizontal displacement are illustrated in Fig. 6. Here, values of soil reactions are plotted as differences of the soil pressures applied on both sides of the specimen at each depth. Spindle-shaped hysteresis curves are observed in the loose soil case (SR-0-L) and the slipping-shaped curves in the dense soil case (SR-0-D). The difference between these shapes comes from the self-supporting capacity of surrounding soil.

3.2 Restoring force and displacement relationships at pile head

Restoring force and horizontal displacement hysteresis curves are shown in Fig. 7 for twelve cases of RX-0-L, RR-(0,2)-L, RR-(0,2,4,V)-D, RR-C-D, RC-0-D, SR-0-L and SR-(0,2)-D. Here, the restoring force refers to the reaction at the pile head due to the applied cyclic displacement. When the elastic specimen was subjected to no vertical load (SR-0-L, SR-0-D), different shapes of

hysteresis loops could be observed, which were similar to those of subgrade reactions of soil acting on the pile surface as illustrated in Fig. 6. The same tendency could be observed in the other cases, especially in RX-0-L and RC-0-D. Here, yielding of specimen is defined by yielding of longitudinal bars. In these cases with no vertical load, restoring forces were kept at approximately the yield load after yielding of the specimens with very large area of hysteresis loops. On the other hand, a gradual decrease in restoring forces could be observed in the cases with some axial loads, especially in RR-4-D with high axial stress level of the specimen, due to geometrical nonlinearity (Maki et al. 2003b). In RR-V-D with alternative axial stresses of 2-4MPa in positive deformation and 2-0MPa in negative deformation, the restoring force and displacement relationship was similar to that in RR-4-D in the positive range and that in RR-0-D in the negative range.

3.3 Deformations and crack distributions of piles

Figure 8 shows the crack distributions for all RC specimens after the surrounding soil is removed (at the loading stage of 100 mm horizontal displacement or that at which the remarkable decrease of horizontal load

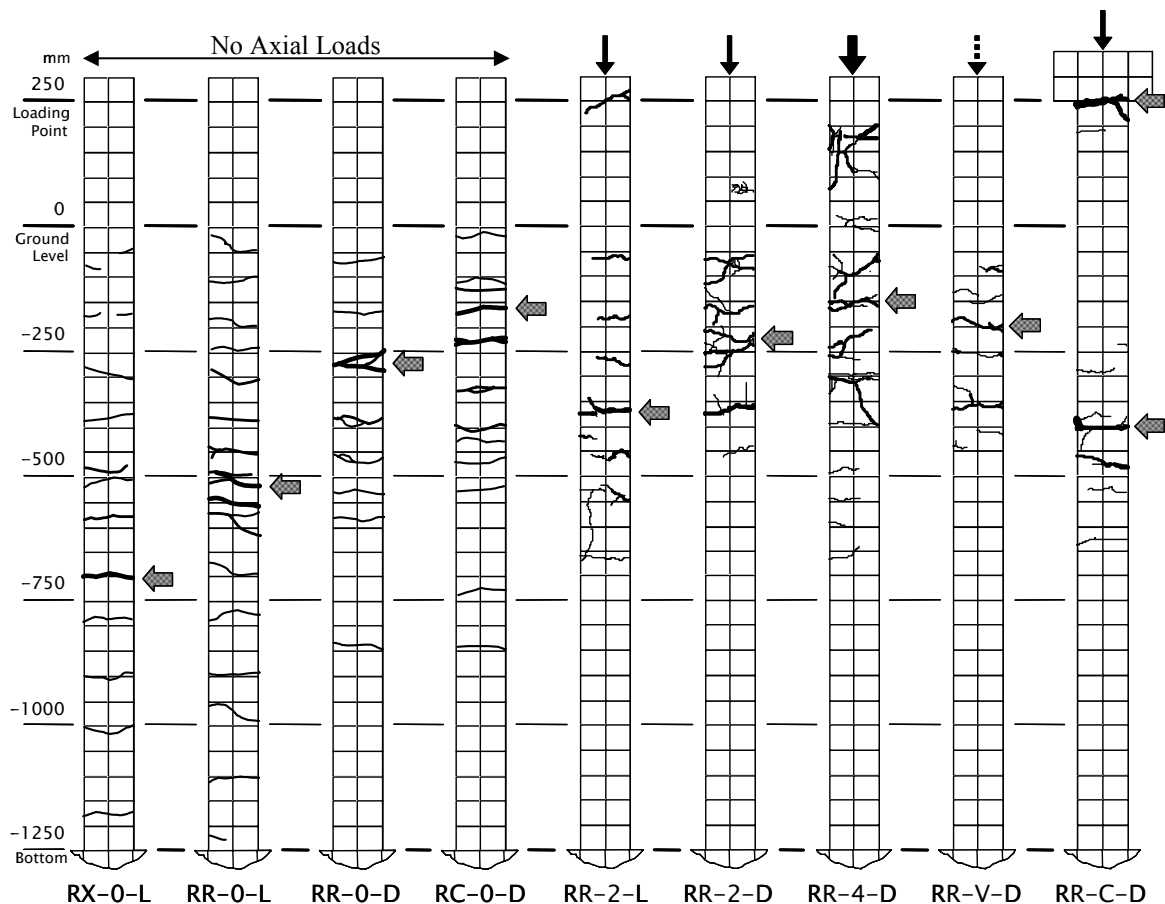


Fig. 8 Crack distributions.

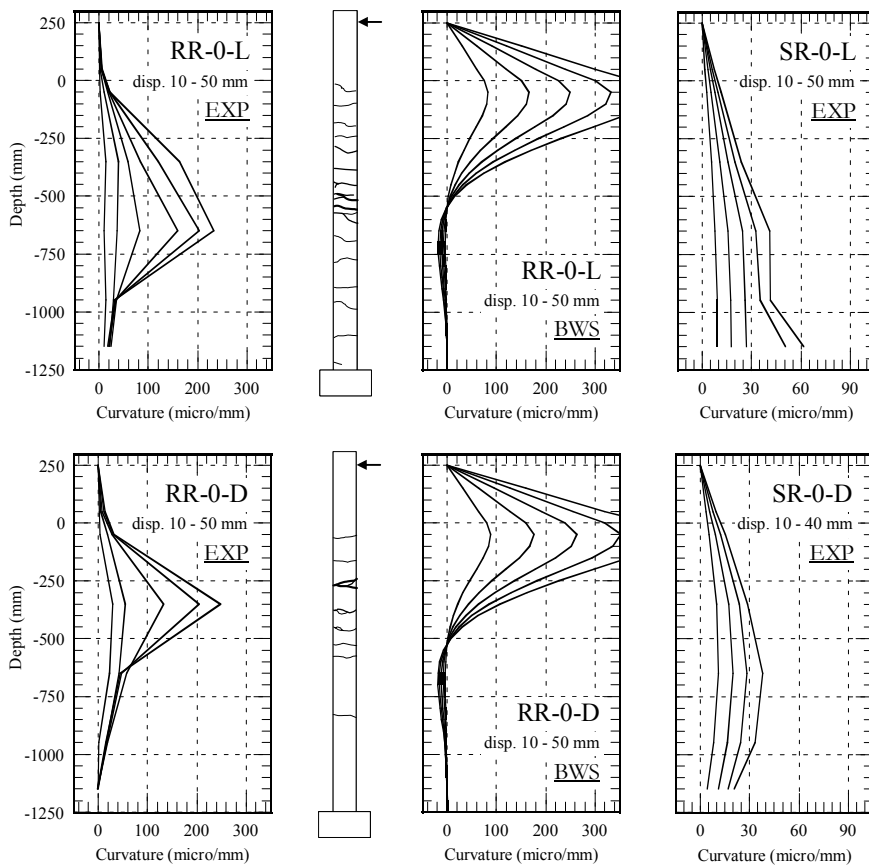


Fig 9 Curvature distributions (RR-0-L and RR-0-D).

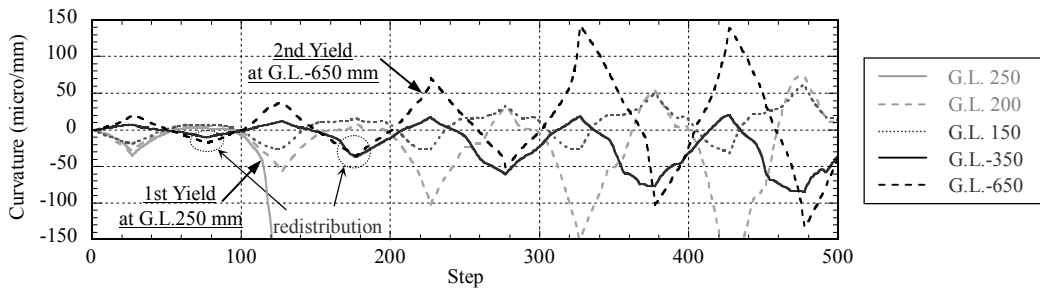


Fig 10 Curvature history (RR-C-D).

could be observed). From the results of four specimens with no axial load (RX-0-L, RR-0-L, RR-0-D and RC-0-D), the maximum damaged depth increases with the increase in the relative stiffness of pile to soil, that is, in RX-0-L, pile with high longitudinal reinforcement ratio embedded in soft soil, large depth of maximum damage point was observed, whereas in RC-0-D, pile with low sectional area embedded in stiff soil, small depth of the point was observed. In addition, cracks were distributed in a wide range of pile in high relative stiffness cases, whereas, cracks were localized at around maximum damaged point in low relative stiffness cases. **Figure 9** shows the curvature distributions drawn by using measured strains on the surface of the specimens

(EXP) and the calculated ones based on the theory of Beam-on-Winkler springs (BWS) with the assumption of constant subgrade soil reaction coefficient independent on depth from ground level, which was proposed by Chang. In this figure, the measured curvature distributions of SR-0-L and SR-0-D are also illustrated together. In the cases of RC pile specimens, the nonlinearity of both reinforced concrete and surrounding soils could be exhibited, but the assumption of Beam-on-Winkler springs was based on the elasticity of pile and soil with constant stiffness, although not initial but yield stiffness of pile was used in the calculation. On the other hand, in the SR series the pile specimens the elasticity of pile specimens could be exhibited, whereas the stiffness of

surrounding soil decreased to the nonlinear deformation domain. These results mean that much higher stiffness of soil is assumed in the calculation based on Beam-on-Winkler springs with Chang's assumption, rather than the stiffness of model soil in the experiment, which resulted in the shallower depth of maximum curvature point. The steel pile specimens used in the SR series had an intermediate stiffness between the initial and yield stiffness of RC pile specimens in RR series, as shown in **Table 2**. Therefore, the maximum deformation in the RR series could be observed at the shallower depth than that in the SR series.

The effect of axial stress levels were considered from these results of (RR-0-L, RR-2-L) and (RR-0-D, RR-2-D, RR-4-D). The maximum damaged depth also depends on the axial stress level, that is to say, the depth becomes small with the increase in axial stress level. In RR-V-D, of which axial stress was varied from 0MPa to 4MPa, where 2MPa of axial stress was applied at pile head displacement of zero, the location of the maximum damaged point was almost the same as in RR-2-D with constant 2MPa axial stress. Moreover, two damaged points could be observed in RR-C-D, in which the rotation at the pile head was confined. The first wide crack occurred at the connections between the pile and small footing at the pile head, and the other at G.L.-400 mm, which was a relatively large depth compared with RR-2-D due to moment redistributions after the first yielding at the pile head. **Figure 10** supports the moment redistributions in RR-C-D, namely, the curvature levels at G.L.-350 mm and G.L.-650 mm are replaced before and after the occurrence of first yielding at G.L.250 mm (pile head).

4. Analytical study using 3-D FEM program

Fundamental datasets of pile behavior in soil media could be achieved from the loading tests as stated in the previous sections. The final objective of this research is to develop the performance evaluation method of the

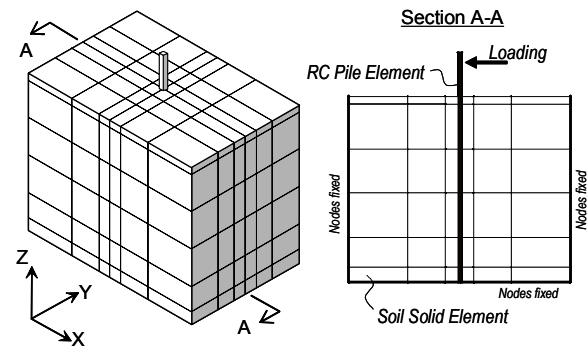


Fig. 11 Finite element modeling of pile-soil system.

pile-soil system with high precision. Therefore, the experimental datasets are utilized for evaluating the applicability of the analytical method for pile-soil systems. The results of simulation using 3-dimensional finite element analysis are discussed in the following sections.

4.1 Finite element modeling and constitutive laws

The analytical investigations in this section were derived by using a 3-dimensional FEM code "COM3" for reinforced concrete structures, which was developed by Prof. Okamura, Prof. Maekawa and their colleagues at the University of Tokyo (Maekawa et al. 1983, Okamura et al. 1991). Described below are the finite element modeling and the material constitutive laws for simulating the experimental results of pile-soil interactions.

The finite element modeling of pile-soil system is shown in **Fig. 11**. RC pile was modeled by 3-D RC beam elements, and 3-D soil solid elements were used for surrounding soil. The nodes at the bottom of the soil were fixed in the Z direction, and those in the side of the model were fixed in the normal directions of the side surfaces. The node at the bottom of the pile was fixed in all translational and rotational directions. These re-

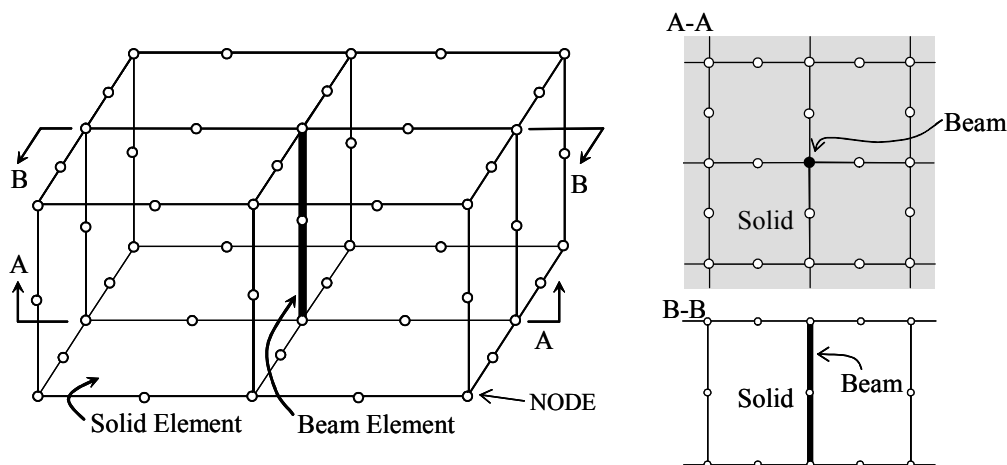


Fig. 12 Configuration of FEM modeling pile and soil using beam and solid element.

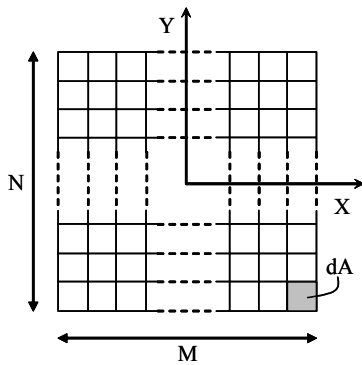


Fig. 13 Cell division in cross section.

flected the boundary conditions in the loading tests. The RC pile elements and the soil elements around the pile used the same nodes that resulted in the pile being perfectly connected to the surrounding soil, that is, the nodes of soil solid elements are connected by beam elements, as shown in Fig. 12. The effect of nonlinear properties between pile and soil has already been discussed in other publications (Maki et al. 2002, Maki et al. 2003a). The loading surface is known as an effective factor on the horizontal behavior of the pile, but in this study, beam elements with no volume were used for modeling pile specimens, intending a decrease in the degree of freedom of the model for the application of the analytical model for the entire structural system. The merits and demerits of this modeling method will be discussed in a subsequent report concerning the com-

parative results of using the beam and solid elements for the pile model.

The applied RC beam elements are formulated based on the flexural theory and fiber model (Tsuchiya et al. 1998). Therefore, the cross section of the element is divided into minute cells (An et al. 1997), as shown in Fig. 13, and axial strain in each cell is calculated from the average axial strain and the two directional curvatures. This strain is transferred to the axial stress by nonlinear constitutive laws of concrete and reinforcement, and the axial force and moments of the element are calculated by integrating the stresses in all cells. Here, shear and torsional deformations are assumed to be linear elastic for the convenience of calculation. For the constitutive laws of concrete and reinforcement, path-dependent average strain-average stress relationships including unloading and reloading paths based on the smeared crack model were applied, and the existing constitutive laws developed by Okamura and Maekawa were incorporated with some modifications. The applied constitutive laws are illustrated in Fig. 14 (Tsuchiya et al. 1998).

In the soil solid element, the stress-strain relationship is divided into the volumetric and deviatoric components, and for the deviatoric component, the hyperbolic type Osaki model is adopted, as shown in Fig. 15. In this model, loading, unloading and reloading paths are prescribed by the relationship of second invariant of deviatoric stress and strain, as formulated in Eq. 1, defined by the initial shear stiffness and shear strength (Ohsaki 1980). This model had already been verified for

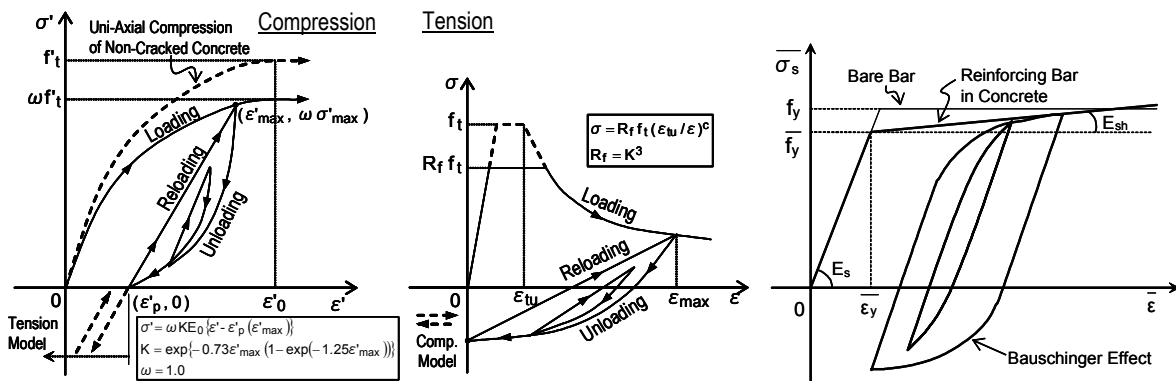


Fig. 14 Nonlinear path-dependent constitutive laws of concrete and reinforcement.

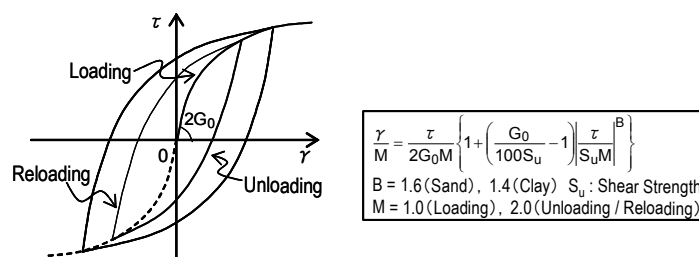


Fig. 15 Nonlinear constitutive laws of soil.

0.001 to 1% shear strain amplitude in the stiffness degradation and the variation of material hysteresis damping (Ohsaki 1980).

$$\frac{J'_2}{M} = \frac{J_2}{2G_0M} \left\{ 1 + \left(\frac{G_0}{100S_u} - 1 \right) \left| \frac{J_2}{S_u M} \right|^B \right\} \quad (1)$$

where,

J_2 : Second invariants of deviatoric stress and strain,

J'_2 : Second invariants of deviatoric stress and strain,

G_0 : Initial shear modulus (N/mm²),

S_u : Shear strength at 1% shear strain (N/mm²),

B : Material parameter (sand: 1.6, clay: 1.4), and

M : Hysteresis parameter

(loading: 1.0, unloading/reloading: 2.0).

Initial shear modulus was calculated with Eq. 2, formulated for Gifu sand used in the experiment (Ishida et al. 1981), and shear strength was evaluated by Coulomb's friction theory, described by Eq. 3.

$$G_0 = 630 \cdot \frac{(2.17 - e)^2}{1 + e} \cdot \sigma_c^{0.321} \quad (2)$$

$$S_u = c \cdot \cos \phi + \sigma_c \cdot \sin \phi \quad (3)$$

where,

e : Void ratio,

σ_c : Confining stress (N/mm²),

c : Cohesion (N/mm²) [= 0.001], and

ϕ : Internal friction angle (deg) [= 27.5].

For sandy soil, variations in relative density (or void ratio) and confining stress strongly affect the static and dynamic behavior of the soil. Additionally, positive and negative dilatancy arises due to repeated shear deformation that results in nonlinear volumetric behavior. However, these nonlinear behaviors were not considered in this analysis.

4.2 Results of FEM simulation

Figure 16 shows the comparison of calculated and measured subgrade soil reaction at each depth. The reactions at G.L.-950 mm could be adequately simulated by the applied analytical model, whereas the reactions at shallower depth were not, especially the area and shape of hysteresis loops. These errors come from the modeling of the interfacial zone around the pile, which is assumed in the analysis as the perfect connection. Therefore, additional analytical studies considering the nonlinear interfacial properties between the pile and soil are needed.

The analytical results of restoring force and displacement relationships in six cases are illustrated in Fig. 17. In each case, the analytical skeleton curve was in good agreement with the experimental curve, especially in the plastic range with load degradation due to the axial load, whereas the analytical hysteresis loops are much smaller than those in experimental result. The errors in hysteresis curves are due to modeling of the pile with no volume beam elements; in other words, the

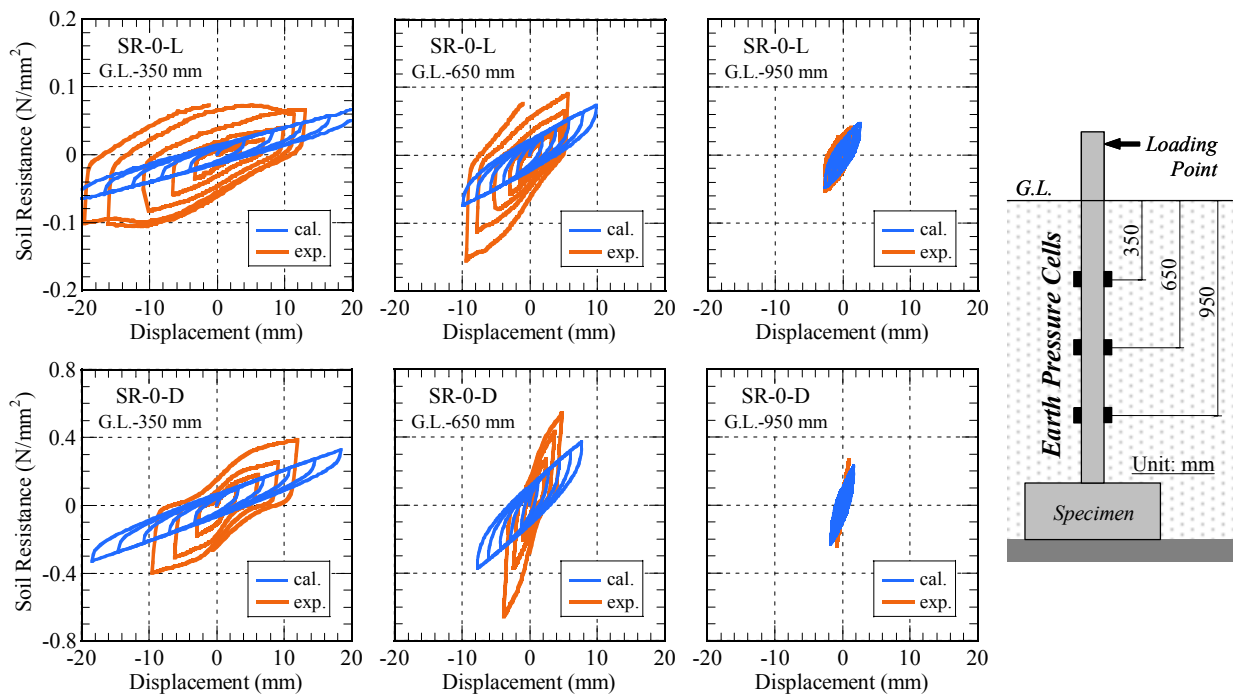


Fig. 16 Computed and measured subgrade soil reactions (SR-0-L and SR-0-D).

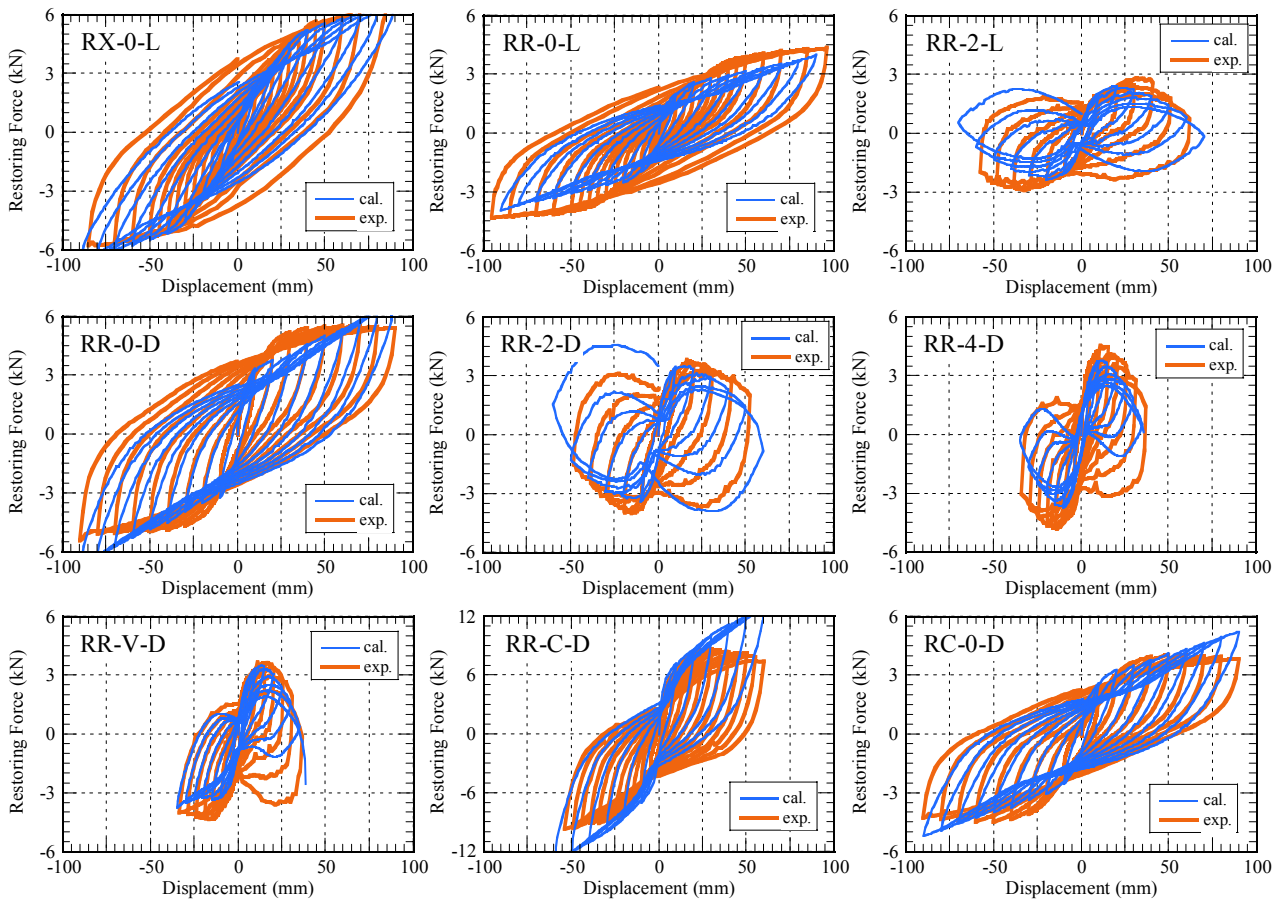


Fig. 17 Computed and measured restoring force - displacement hysteresis curves.

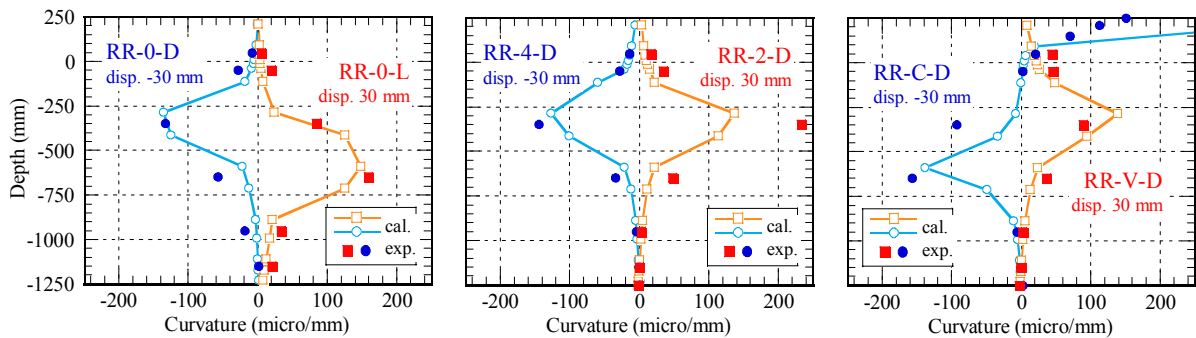


Fig. 18 Computed and measured curvature distributions.

local nonlinear behavior of soil around the pile cannot be well simulated by a model with no volume elements, and localized tensile stresses exist between the pile and soil, according to the applied soil material model of the linear elastic volumetric stress-strain relationship. Therefore, further investigations applying a complete 3-D solid element model for RC piles are needed.

Figure 18 shows comparisons between the analytical and experimental curvature distributions of the pile at horizontal displacement of 30 mm at the pile head. The

shapes of curvature distributions of piles and the locations of plastic hinges can be simulated by the applied analytical method. In RR-C-D, a difference between computed and observed curvatures near the pile head can be seen. It is supposed that the pull-out of longitudinal reinforcement from footing at the pile head is remarkable in the experiment, a fact that was not considered in the analysis. As a result, the measured curvature is much lower than that calculated in the analysis.

5. Conclusions

In this paper, experimental and analytical investigations were conducted in order to clarify the behavior of reinforced concrete piles under ground when the pile is subjected to a large plastic deformation. Following conclusions could be drawn from these investigations:

- 1) The location, at which maximum curvature or maximum damage is observed, is dependent on the relative stiffness between the pile and its surrounding soil. The axial load results in the higher stiffness of a pile than piles of no axial force. Therefore, the higher the axial load is, the shallower the depth of maximum damage of a pile.
- 2) The restoring force degradations and large area of hysteresis loops in large plastic deformation range could be observed in the cases with some axial loads compared with the cases with no axial load, due to the geometrical nonlinearity or P- δ effects.
- 3) The adopted FEM analysis can simulate the experimental behavior of restoring force-displacement skeleton curve and deformation of a pile, but as to hysteresis behavior, further investigations are needed.

Acknowledgements

The FEM code COM3 was offered by Prof. Koichi Maekawa of the University of Tokyo. The authors wish to acknowledge his kind cooperation. Additionally, the cooperation of the members of the structural material laboratory in Saitama University for experimental work is also gratefully acknowledged.

References

- An, X., Maekawa, K. and Okamura, H. (1997). "Numerical Simulation of Size Effect in Shear Strength of RC Beams." *Journal of Materials, Concrete Structures and Pavements*, JSCE, No. 564/V-35, 297-316.
- Chai, Y. H. and Hutchinson, T. C. (2002). "Flexural Strength and Ductility of Extended Pile-Shafts, I: Analytical Model and II: Experimental Study." *Journal of Structural Engineering*, ASCE, 128 (5), 586-602.
- Fukui, J., Kimura, Y., Ohkoshi, M. and Banno, A. (1998). "Cyclic Lateral Loading Tests for Single Pile in Sandy Ground." *Civil Engineering Techniques*, 40 (3), 62-67. (in Japanese).
- Ishida, T. et al. (1981). "Static and Dynamic Mechanical Properties of Materials for Model Tests (Gifu sand) under Low Confining Stress." *Research Report of Electrical Power Center Research Institute*, No. 380045. (in Japanese).
- JSCE, (2002). "Standard Specification for Design and Construction of Concrete Structures [Seismic Performance Evaluation]." Tokyo: Japan Society of Civil Engineers.
- Maekawa, K. and Okamura, H. (1983). "The Deformational Behavior and Constitutive Equation of Concrete using Elasto-Plastic and Fracture Model." *Journal of Faculty of Engineering*, University of Tokyo (B), 37 (2), 253-328.
- Maki, T. and Mutsuyoshi, H. (2000). "Response Behavior of RC Piles under Severe Earthquake." *Proceedings of the 12th World Conference on Earthquake Engineering [CD-ROM]*, Auckland, New Zealand, February 2000.
- Maki, T. and Mutsuyoshi, H. (2001). "Restoring Force and Deformation of Reinforced Concrete Piles." *Journal of Materials, Concrete Structures and Pavements*, JSCE, No. 683/V-52, 103-118. (in Japanese).
- Maki, T. and Mutsuyoshi, H. (2002). "Study on Seismic Performance of Reinforced Concrete Piles under Ground." In: K. Kawashima, I. G. Buckle and C-H. Loh, Eds. *Proceedings of the 3rd International Workshop on Performance-Based Seismic Design and Retrofit of Transportation Facilities (Technical Report TIT/EERG 02-2)*, Tokyo, Japan, 9-11 July 2002. Tokyo: Tokyo Institute of Technology, 67-78.
- Maki, T. and Mutsuyoshi, H. (2003a). "Effect of Local Characteristics between Pile and Soil on Seismic Behavior of RC Piles under Ground." *Proceedings of fib 2003 Symposium on Concrete Structures in Seismic Regions [CD-ROM]*, Athens, Greece, 6-8 May 2003.
- Maki, T., Okitsu, M., Nakamura, M. and Mutsuyoshi, H. (2003b). "Effect of Geometrical Nonlinearity on the Response Behavior of RC Piles under Ground." *Proceedings of the Japan Concrete Institute*, 25 (2), 1387-1392. (in Japanese).
- Ohsaki, Y. (1980). "Some Notes on Masing's Law and Nonlinear Response of Soil Deposits." *Journal of Faculty of Engineering*, University of Tokyo (B), 35 (4), 513-536.
- Okamura, H. and Maekawa, K. (1991). "Nonlinear Analysis and Constitutive Models of Reinforced Concrete." Tokyo: Gihodo Shuppan.
- Tsuchiya, S., Fukuura, N. and Maekawa, K. (1998). "Dynamic Response of RC Piers applied with Multi-Directional Forces using 3-Dimensional FEM Analysis based on Fiber Model." *Proceedings of the JCI Symposium on Deterioration of Concrete Members in the Plastic Yielding Stage under Cyclic Seismic Overload*, Tokyo, Japan, 20-21 August 1998. Tokyo: Japan Concrete Institute, 359-368. (in Japanese).